

1 Re-examination of C<sub>1</sub>-C<sub>5</sub> alkyl nitrates in Hong Kong using an observation-based  
2 model

3 X.P. Lyu<sup>1</sup>, Z.H. Ling<sup>1,2</sup>, H Guo<sup>1\*</sup>, S.M. Saunders<sup>3</sup>, S.H.M. Lam<sup>3,4</sup>, N. Wang<sup>1</sup>, Y. Wang<sup>1</sup>, M. Liu<sup>1</sup>,  
4 T Wang<sup>1</sup>

5 <sup>1</sup> Department of Civil and Environmental Engineering, The Hong Kong Polytechnic University,  
6 Hong Kong

7 <sup>2</sup> Department of Atmospheric Science, School of Environmental Science and Engineering, Sun  
8 Yat-sen University, China

9 <sup>3</sup> School of Chemistry and Biochemistry, University of Western Australia, Perth, Western  
10 Australia, Australia

11 <sup>4</sup> Pacific Environment Limited, Perth, Western Australia, Australia

12 **Abstract:** The photochemical formation of alkyl nitrates (RONO<sub>2</sub>) and their impact on ozone  
13 (O<sub>3</sub>) formation were investigated using a Photochemical Box Model incorporating the Master  
14 Chemical Mechanism (PBM-MCM). The model was constrained with field measurement data  
15 collected on selected O<sub>3</sub> episode days at Tai O, a rural-coastal site in southwestern Hong Kong,  
16 from August 2001-December 2002. The in-situ observations showed that the sum of C<sub>1</sub>-C<sub>5</sub>  
17 RONO<sub>2</sub> varied from 30.7±14.8 pptv in spring to 120.7±10.4 pptv in autumn, of which 2-butyl  
18 nitrate dominated with the highest average concentration of 30.8±2.6 pptv. Model simulations  
19 indicated that the pathway of CH<sub>3</sub>O reacting with NO<sub>2</sub>, proposed in our previous study, made  
20 minor contributions (11.3±0.7%) to methyl nitrate formation. Indeed, 51.8±3.1% and 36.5±6.3%  
21 of the methyl nitrate was attributed to the reaction of CH<sub>3</sub>O<sub>2</sub>+NO and to oceanic  
22 emissions/biomass burning, respectively. For the C<sub>2</sub>-C<sub>5</sub> alkyl nitrates, the contribution of  
23 photochemical formation increased with increasing carbon number, ranging from 64.4±4.0% for  
24 ethyl nitrate (EtONO<sub>2</sub>) to 72.6±4.2% for 2-pentyl nitrate (2-PenONO<sub>2</sub>), while the contribution of  
25 oceanic emissions/biomass burning decreased from 35.1±6.5% for EtONO<sub>2</sub> to 26.8±6.8% for 2-  
26 PenONO<sub>2</sub>. Model simulations of photochemical O<sub>3</sub> levels influenced by RONO<sub>2</sub> chemistry  
27 showed that the formation of methyl-, ethyl-, *i*-propyl-, *n*-propyl-, 2-butyl-, 2-pentyl-, and 3-  
28 pentyl-nitrates led to O<sub>3</sub> reduction of 0.05±0.03, 0.05±0.03, 0.06±0.02, 0.02±0.02, 0.18±0.04,

\*Corresponding author. Tel: 852 3400 3962; Fax: 852 2334 6389; Email: ceguohai@polyu.edu.hk 1

29 0.09±0.02 and 0.06±0.02 ppbv, respectively, with an average reduction rate of 11.0±3.2 ppbv O<sub>3</sub>  
30 per 1 ppbv RONO<sub>2</sub> formation. The C<sub>1</sub>-C<sub>5</sub> RONO<sub>2</sub> constituted 18.6±1.9% of the entire RONO<sub>2</sub>,  
31 and had a nitrogen reserve of 4.1±0.2%, implying their potential influence on O<sub>3</sub> production in  
32 downwind areas.

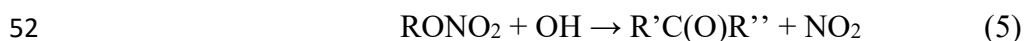
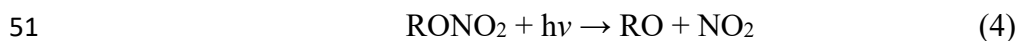
33 **Keywords:** alkyl nitrate; photochemical formation; O<sub>3</sub> production; PBM-MCM model; field  
34 observation

35

## 36 1. Introduction

37 Photochemical pollution characterized by elevated O<sub>3</sub> in the troposphere (Guo et al., 2013a;  
38 Wang et al., 2009) is of increasing concern in megacities, such as the city cluster in the Pearl  
39 River Delta (PRD) region, where huge emissions of O<sub>3</sub> precursors, *i.e.*, volatile organic  
40 compounds (VOCs) and nitrogen oxides (NO<sub>x</sub>) from industries and traffic have caused intense  
41 periods of high photochemical O<sub>3</sub> formation (Cheng et al., 2010; Ling et al., 2011) notably in the  
42 autumn period. Alkyl nitrates (RONO<sub>2</sub>) are formed as byproducts in the process of O<sub>3</sub> formation,  
43 and are also temporary reservoirs of nitrogen. However, to date there have been few studies on  
44 the influence of individual alkyl nitrate on the O<sub>3</sub> budget (Wang et al., 2013; Williams et al.,  
45 2014).

46 There are 5 key gas phase reactions in the troposphere, (1)–(5), for the production and  
47 destruction of alkyl nitrates:



53 The photochemical formation of RONO<sub>2</sub> is mainly attributed to reactions (1) and (2) (Atkinson  
54 et al., 1982; Wang et al., 2013). Alternative pathways, *i.e.*, reactions between organic aerosols  
55 and particle-phase nitrates, and NO<sub>3</sub> initiated oxidation of RO<sub>2</sub> at nighttime, also contribute to

56 photochemical RONO<sub>2</sub> production (Worton et al., 2010). Studies (Jenkin et al., 2000; Suarez-  
57 Bertoa et al., 2012) indicate that reaction (1) contributes most to ambient RONO<sub>2</sub> and becomes  
58 increasingly important with increasing carbon number of the RO<sub>2</sub> species, because the  
59 decomposition rate of the vibrationally-excited RONO<sub>2</sub> decreases with increased complexity of  
60 the alkyl (R) group, hence the survival of stabilized RONO<sub>2</sub> increases (Atkinson et al., 1983). If  
61 the vibrationally-excited RONO<sub>2</sub> is not formed, an oxygen atom (O) exchange between RO<sub>2</sub> and  
62 NO will occur, *i.e.*, reaction (3). The branching ratio ( $\alpha$ ) is often used to define the relative  
63 reactivity of reaction (1) competing with the reaction (3) (Flocke et al., 1998; Farmer et al.,  
64 2011). In contrast to the formation pathway of reaction (1), the production efficiency of RONO<sub>2</sub>  
65 from reaction (2), *i.e.*, RO+NO<sub>2</sub>, decreases with increasing carbon number because of the  
66 increasing tendency of isomerization and decomposition of RO, and relatively lower abundance  
67 of RO compared to the methoxy radical (CH<sub>3</sub>O) as the carbon number increases (Atkinson et al.,  
68 1982; Williams et al., 2014).

69 As well as photochemical formation, equatorial oceans (Atlas et al., 1993; Blake et al., 2003)  
70 are a primary source of ambient RONO<sub>2</sub>, particularly for light (<C<sub>2</sub>) RONO<sub>2</sub>. Blake et al. (2003)  
71 reported that methyl nitrate (MeONO<sub>2</sub>) was significantly emitted from tropical and subtropical  
72 oceans, which was an important source of excess MeONO<sub>2</sub> that cannot be explained by  
73 photochemical formation. Additionally, biomass burning is also a source of RONO<sub>2</sub>, for which  
74 Simpson et al. (2002) proposed a formation mechanism in the combustion stage involving the  
75 combination of RO<sub>2</sub> to generate RO and the reaction of RO with NO<sub>2</sub>.

76 Since RONO<sub>2</sub> are formed simultaneously with O<sub>3</sub>, they are good tracers of photochemical  
77 pollution (Simpson et al., 2006; Aruffo et al., 2014). They also affect O<sub>3</sub> production by  
78 interfering with the NO<sub>x</sub> budget as temporary nitrogen reservoirs (Aruffo et al., 2014). The  
79 availability of reactive nitrogen will be reduced through reactions (1) and (2) due to the long  
80 atmospheric lifetimes of RONO<sub>2</sub> (Atlas, 1988). Moreover, the RO generated from reaction (3)  
81 decreases, resulting in the loss of OH and HO<sub>2</sub>. These will reduce the potential for O<sub>3</sub> production.  
82 On the other hand, the formation of RONO<sub>2</sub> competes with the reaction of O<sub>3</sub> titration by NO. As  
83 a temporary reservoir of reactive NO<sub>x</sub>, RONO<sub>2</sub> can also release RO and NO<sub>2</sub> through photolysis  
84 (reaction (4)) and OH-initiated oxidation (reaction (5)) (Aschmann et al., 2011; He et al., 2011).  
85 The additional NO<sub>2</sub>, secondary organic degradation products (*i.e.*, PANs, aldehydes, ketones, etc.)

86 and radicals (*i.e.*, RO<sub>2</sub>, HO<sub>2</sub>, OH, etc.) consequently promote the photochemical production of O<sub>3</sub>.  
87 During the process of RONO<sub>2</sub> degradation, OH and HO<sub>2</sub> are consumed and their recycling is  
88 strongly dependent on the reactivity of the carbonyls generated from the oxidation of RO  
89 ([Derwent et al., 2005](#)). It remains uncertain whether RONO<sub>2</sub> make positive or negative  
90 contributions to O<sub>3</sub> formation, and what differences there are between individual alkyl nitrate  
91 species.

92 In this study, PBM-MCM model was adapted to investigate the photochemical formation of  
93 C<sub>1</sub>-C<sub>5</sub> RONO<sub>2</sub> and their impacts on O<sub>3</sub> production at Tai O, a rural-coastal site in southwestern  
94 Hong Kong. Using the same dataset, [Simpson et al. \(2006\)](#) reported the mixing ratios and  
95 seasonal patterns of the observed RONO<sub>2</sub>, the potential formation pathways of MeONO<sub>2</sub> and the  
96 correlation between the sum of C<sub>1</sub>-C<sub>5</sub> RONO<sub>2</sub> and O<sub>3</sub>. Here alternative formation pathways of  
97 MeONO<sub>2</sub> were examined, and the correlations between RONO<sub>2</sub> and O<sub>3</sub> were fully developed by  
98 quantifying the impacts of the C<sub>1</sub>-C<sub>5</sub> RONO<sub>2</sub> formation on the net O<sub>3</sub> production.

99

## 100 **2. Experimental**

### 101 **2.1 Sample collection and chemical analysis**

102 From 24<sup>th</sup> Aug. 2001 to 31<sup>st</sup> Dec. 2002, a multi-pollutant sampling campaign was conducted at  
103 Tai O, a rural-coastal site in southwestern Hong Kong. [Figure 1](#) shows the geographical location  
104 of the sampling site (22.25°N, 113.85°E). Local emissions are not predominant at this site due to  
105 the low traffic and population density. Tai O is located approximately 30 km to the west of the  
106 urban center of Hong Kong, 30 km to the east of Macau, and at the mouth of Pearl River Estuary.  
107 This site is influenced by air pollution from the PRD region, particularly enhanced in the cooler  
108 autumn-winter seasons when northeastern winds passing over the PRD region and Hong Kong  
109 urban areas dominate. Conversely, air pollution from the PRD is less evident during the  
110 prevailing summer southerly winds bringing in fresh air and diluting the air pollution. Full  
111 details about the sampling site and field campaign are available in [Wang et al. \(2005\)](#) and  
112 [Simpson et al. \(2006\)](#).

113

114 Figure 1. Geographical location of the Tai O sampling site and environs. The red star = Tai O, orange  
115 blocks = urban areas, and pink dots represent the population distributions.

116 Whole air VOC samples were collected using evacuated 2-L stainless steel canisters, which  
117 were preprocessed with 10 Torr of degassed, distilled water to quench the active surface sites of  
118 the inner walls. The canisters were cleaned and evacuated following the procedures described in  
119 [Simpson et al. \(2006\)](#) prior to sampling. Each whole air sample was collected through a valve for  
120 1 min. to ensure that the canister was fully filled. After sampling, the canisters were shipped to  
121 the University of California, Irvine (UCI) for chemical analysis. Totally, mixing ratios of 7 C<sub>1</sub>-C<sub>5</sub>  
122 RONO<sub>2</sub>, 42 nonmethane hydrocarbons (NMHCs), 26 halocarbons and 3 reduced sulfur  
123 compounds were determined. Details on the analysis techniques, detection limits and quality  
124 control strategies are given in [Colman et al. \(2001\)](#) and [Simpson et al. \(2006\)](#). It is important to  
125 note that the RONO<sub>2</sub> were calibrated with a new scale in 2008 that applied a factor of 2.13, 1.81,  
126 1.24, 1.17 and 1.13 to C<sub>1</sub>, C<sub>2</sub>, C<sub>3</sub>, C<sub>4</sub> and C<sub>5</sub> RONO<sub>2</sub>. This scale was provided by Atlas  
127 (University of Miami), and accepted by the analytical team (UCI) ([Simpson et al., 2011](#)).

128 The measurement techniques for trace gases, *i.e.*, CO, NO, NO<sub>y</sub>, SO<sub>2</sub> and O<sub>3</sub> are fully  
129 described in [Wang et al. \(2003a\)](#). Briefly, CO was thermally catalyzed to CO<sub>2</sub>, and then  
130 measured with a gas filter correlation, non-dispersive infrared analyzer (Advanced Pollution  
131 Instrumentation, Inc., Model 300); NO and NO<sub>y</sub> were detected with a modified commercial  
132 MoO/chemiluminescence analyzer (Thermo-Environmental Instruments, Inc. (TEI), Model 42S)  
133 that converted NO<sub>y</sub> to NO on the surface of MoO, and then NO was quantified by the  
134 chemiluminescent analyzer; SO<sub>2</sub> was measured by pulsed UV fluorescence (TEI, Model 43S);  
135 and a commercial UV photometric instrument (TEI, Model 49) was used to detect the O<sub>3</sub> mixing  
136 ratios. The detection limits of CO, NO, NO<sub>y</sub>, SO<sub>2</sub> and O<sub>3</sub> were 30, 0.05, 0.05, 10 and 2 ppbv,  
137 respectively.

## 138 2.2 Model description

### 139 2.2.1 PMF model

140 Based on the chemical mass balance between measured species concentrations and source  
141 profiles, Positive Matrix Factorization (PMF) treats the measured concentration of species, *j*, in  
142 sample *i* ( $x_{ij}$ ) as the sum of contributions from *p* sources, which can be decomposed as

143 contribution,  $G$  and source profile,  $F$ , as shown in the following equation (eqn. 1): (Paatero,  
144 1997):

$$145 \quad x_{ij} = \sum_{k=1}^p g_{ik} f_{kj} + e_{ij} \quad \text{eqn. 1}$$

146 where  $g_{ik}$  is the species contribution of the  $k$ th source to the  $i$ th sample,  $f_{kj}$  is the species fraction  
147 in the  $k$ th source and  $e_{ij}$  is the residual associated with species  $j$  in sample  $i$ . Details on the PMF  
148 operation is provided in Guo et al. (2011).

### 149 2.2.2 PBM-MCM model

150 The PBM-MCM is a photochemical box model combined with a near-explicit chemical  
151 mechanism, which has been successfully applied in previous studies (Lam et al., 2013; Ling et  
152 al., 2014). Details on the model construction can be found in Lam et al. (2013) and the  
153 mechanism in Saunders et al. (2003) and Jenkin et al. (2003). Briefly, field measurement data,  
154 *i.e.*, VOCs, SO<sub>2</sub>, CO, NO, NO<sub>2</sub>, O<sub>3</sub>, temperature and relative humidity, are used to construct the  
155 model. The model considers photochemical processes appropriate to the planetary boundary  
156 layer (PBL) and comprises the chemical mechanism (MCMv3.2) involving around 5,900 species  
157 and 16,500 reactions. The reactions are homogeneous in the boundary layer and no vertical/  
158 horizontal dispersion is considered. To achieve appropriate simulation for the region, the model  
159 has been developed and adjusted for Hong Kong (Lam et al., 2013; Ling et al., 2014). For  
160 example, the boundary layer is set to vary between 300-1400 m according to actual autumn  
161 conditions in Hong Kong, while the photolysis rates are determined using the photon fluxes from  
162 the Tropospheric Ultraviolet and Visible Radiation (TUVv5) Model (Madronich and Flocke,  
163 1997) as a function of the location of Hong Kong and time period of the campaign. The  
164 concentrations of stable species above the boundary layer, *i.e.*, RONO<sub>2</sub>, peroxyacetyl nitrate-type  
165 compounds (PANs) and carbonyls, are set based on the previous application of the model in  
166 Hong Kong (Lam et al., 2013). These species exist in the aloft layer (the free troposphere above  
167 PBL) and are entrained in PBL during the morning as the boundary layer expands. However, this  
168 is a natural mixing process involving molecular movement, but not physical process like wind or  
169 vertical exchange. Further details can be found in Lam et al. (2013).

170 In this study, the field observations of 69 parameters consisting of 2 meteorological factors  
171 (*i.e.*, temperature and relative humidity), 5 trace gases (*i.e.*, SO<sub>2</sub>, CO, O<sub>3</sub>, NO and NO<sub>2</sub>), 61 non-

172 methane VOCs and CH<sub>4</sub> were used to constrain the model. Five O<sub>3</sub> episode days (*i.e.*, 11<sup>th</sup> and  
173 25<sup>th</sup> Oct., 2002 and 06<sup>th</sup>-08<sup>th</sup> Nov. 2002) were selected from the whole sampling campaign, in  
174 order to study the photochemical formation of C<sub>1</sub>-C<sub>5</sub> RONO<sub>2</sub> and their impacts on net O<sub>3</sub>  
175 production. The hourly data required for the PBM-MCM input were only available on these 5  
176 days, and they are representative of autumn conditions when high photochemical pollution  
177 frequently occurs. The first hourly (*i.e.*, 07:00) data were used to initiate the model simulations.  
178 The model was run in a base case (BC) and two constrained cases (CC<sub>1</sub> and CC<sub>2</sub>). Details on the  
179 model configuration are provided in Table 1.

180 Table 1 Model configuration of the base case and constrained cases

181  
182 It is noteworthy that NO<sub>2</sub> was obtained from the difference between NO and NO<sub>y</sub>, because NO<sub>y</sub>  
183 detected by the MoO/chemiluminescence analyzer approximately equals NO<sub>x</sub> when the air mass  
184 is greatly affected by fresh emissions (Xu et al., 2013). In this study, ~90% of air masses were  
185 identified as freshly emitted polluted air, with ethyne/CO > 4 pptv/ppbv according to the method  
186 proposed by Smyth (1996). In addition, the ratios of propane/ethane (1.3±0.2), ethene/ethane  
187 (0.9±0.1) and toluene/benzene (7.4±0.6) at Tai O on the five episode days were comparable to  
188 those at an urban site in Hong Kong (1.0±0.1, 1.1±0.1 and 7.3±1.2 for propane/ethane,  
189 ethene/ethane and toluene/benzene, respectively) (Guo et al. 2007), further confirming that Tai O  
190 was significantly influenced by fresh emissions during the episodes. Furthermore, PANs and  
191 RONO<sub>2</sub> were only ~7% of NO<sub>2</sub>, as indicated in section 3.3.2 “Nitrogen partitioning”. Therefore,  
192 the slightly-overestimated NO<sub>2</sub> would not significantly influence RONO<sub>2</sub> formation.

193

### 194 3. Results and discussion

#### 195 3.1 Mixing ratios and seasonal patterns of RONO<sub>2</sub>

196 Table 2 shows the mean levels of O<sub>3</sub>, C<sub>1</sub>-C<sub>5</sub> RONO<sub>2</sub> and their parent hydrocarbons at Tai O  
197 over the whole sampling period, with 95% confidence intervals. It was found that the average  
198 mixing ratios of RONO<sub>2</sub> ranged from 4.0±0.4 pptv for *n*-PrONO<sub>2</sub> to 30.8±2.6 pptv for 2-  
199 BuONO<sub>2</sub>. Inconsistently, the *n*-butane mixing ratio (1893±586 pptv) was the second lowest

200 among the parent hydrocarbons, while the parent hydrocarbon of *n*-PrONO<sub>2</sub> (*i.e.* propane)  
201 ranked the second highest with an average mixing ratio of 2392±740 pptv. This suggested that  
202 RONO<sub>2</sub> not only relates to the abundance, but also the reaction pathways and reactivity of the  
203 parent hydrocarbon (Atlas et al., 1993; Blake et al., 2003), as well as primary emissions.

204 Similar seasonal patterns were observed for the sum of C<sub>1</sub>-C<sub>5</sub> RONO<sub>2</sub> and O<sub>3</sub>, *i.e.*, higher in  
205 autumn and lower in spring, suggesting the importance of photochemical formation of RONO<sub>2</sub>.  
206 The average mixing ratios of the sum of C<sub>1</sub>-C<sub>5</sub> RONO<sub>2</sub> were 30.7±14.8, 74.9±23.8, 120.7±10.4  
207 and 91.2±8.8 pptv in spring, summer, autumn and winter, respectively. Similar to RONO<sub>2</sub>, the  
208 average mixing ratio of O<sub>3</sub> also peaked in autumn (68.4 ± 8.0 ppbv). Indeed, the sum of C<sub>1</sub>-C<sub>5</sub>  
209 RONO<sub>2</sub> correlated well with O<sub>3</sub> (R<sup>2</sup> = 0.71), and for MeONO<sub>2</sub> (R<sup>2</sup> = 0.62). However, inconsistent  
210 with the observation that O<sub>3</sub> had lowest mixing ratios in winter (25.1±5.7 ppbv), RONO<sub>2</sub> levels  
211 in winter were the second highest among the four seasons (91.2±8.8 pptv), implying possible  
212 RONO<sub>2</sub> sources from oceanic emissions and/or biomass burning. Therefore, the pathway  
213 contributions to RONO<sub>2</sub> were determined in the following section (3.2).

214 Table 2 Statistics of C<sub>1</sub>-C<sub>5</sub> RONO<sub>2</sub> and O<sub>3</sub> at Tai O over the whole sampling period (mean±95%  
215 confidence interval) (units: pptv unless otherwise specified)

### 216 3.2 Pathways to RONO<sub>2</sub>

217 Since the PBM-MCM is a chemical model without the consideration of primary emissions, the  
218 primary emission of RONO<sub>2</sub> should be eliminated before the model simulation. Here, the hourly  
219 C<sub>1</sub>-C<sub>5</sub> RONO<sub>2</sub> mixing ratios were applied in PMF analysis for source apportionment (Guo et al.,  
220 2013b). Figure 2 shows the profiles of three sources extracted by PMF. Factor 1 is distinguished  
221 by high loadings of O<sub>3</sub> and RONO<sub>2</sub>, likely to represent the secondary formation of RONO<sub>2</sub>.  
222 Additionally, moderate percentages of methyl chloride (CH<sub>3</sub>Cl) were observed in this factor.  
223 Apart from oceanic sources, CH<sub>3</sub>Cl can be emitted from biomass burning (Rudolph et al., 1995),  
224 another source of RONO<sub>2</sub>. Although RONO<sub>2</sub> is formed secondarily in the combustion stage of  
225 biomass burning, its formation mechanism is quite different from that in the normal atmosphere  
226 (Simpson et al., 2002). Therefore, CH<sub>3</sub>Cl in this factor may indicate RONO<sub>2</sub> formation in the  
227 stage of plume transport, rather than RONO<sub>2</sub> formed in the combustion stage of biomass burning.  
228 Factor 2 has high loadings of dimethyl sulfide (DMS) and bromoform (CHBr<sub>3</sub>), which are  
229 typical tracers of marine outflows (Nowak et al., 2001; Atlas et al., 1993). In addition, the



230 moderate percentages of CH<sub>3</sub>Cl and C<sub>2</sub>-C<sub>5</sub> hydrocarbons may indicate RONO<sub>2</sub> formed in the  
231 combustion stage of biomass burning. Therefore, this factor is assigned to be the source of  
232 marine and biomass burning. Factor 3 shows weak associations with RONO<sub>2</sub>, with the  
233 dominance of anthropogenic VOCs. However, DMS also has a high loading in this factor, which  
234 may imply the mixture of marine flows with anthropogenic emissions. This is not unreasonable  
235 given that Tai O is a coastal site adjacent to the South China Sea (see Figure 1). As such, RONO<sub>2</sub>  
236 in factor 3 is thought to be associated with oceanic emissions as well as anthropogenic emissions.

237

238 **Figure 2 Profiles for the sources of RONO<sub>2</sub> at Tai O. The errors were estimated with the Bootstrap**  
239 **method integrated in PMF.**

240 With the exclusion of oceanic sources and biomass burning, the secondarily/photochemically  
241 formed RONO<sub>2</sub> was used to construct and constrain the PBM-MCM model. [Figure 3](#) presents the  
242 simulated and observed O<sub>3</sub> and secondary RONO<sub>2</sub>. It can be seen that the model reasonably  
243 simulated the variations of daytime O<sub>3</sub> and RONO<sub>2</sub>, *i.e.*, the values increased in the morning,  
244 peaked in early afternoon and decreased in late afternoon. The simulated results well captured  
245 the observed low and high values (standard deviation, SD < ±30%) except for O<sub>3</sub>, MeONO<sub>2</sub> and  
246 *n*-PrONO<sub>2</sub> on November 7, 2002 when the simulated maximums were ~ 40%-50% lower than  
247 the observations. This may be caused by the source apportionment of RONO<sub>2</sub> and O<sub>3</sub> by PMF,  
248 which averaged the hourly contributions of each factor, and may underestimate/overestimate the  
249 extremely high/low values. In addition, for most cases, the model simulations did not well track  
250 the rapid decrease of RONO<sub>2</sub> in the afternoon, probably due to the fact that the physical  
251 processes, *i.e.*, vertical and horizontal dispersion were not considered in the PBM-MCM model  
252 ([Lam et al., 2013](#); [Ling et al., 2011](#)).

253

254 **Figure 3 Simulated and observed O<sub>3</sub> and secondary RONO<sub>2</sub> at Tai O on episode days.**

255 To further evaluate the model performance, the index of agreement (IOA) was used to  
256 examine the correlation between simulated and observed results ([Wang et al., 2015](#); [Jiang et al.,](#)  
257 [2010](#)). The IOA value is between 0 and 1, and a higher IOA represents better agreement. The  
258 IOA is determined as follows ([Huang et al., 2005](#)):

259 
$$\text{IOA} = 1 - \frac{\sum_{i=1}^n (O_i - S_i)^2}{\sum_{i=1}^n (|O_i - \bar{O}| + |S_i - \bar{O}|)^2}$$

260 where  $O_i$ ,  $S_i$ , and  $\bar{O}$  refer to the hourly observed value, simulated value, and the average  
 261 observed value, respectively.

262 **Table 3** summarizes the IOAs for the simulation of  $O_3$  and  $C_1$ - $C_5$   $\text{RONO}_2$ . Good to moderate  
 263 agreements were found between the simulated and observed values, indicating the performance  
 264 of this model was reasonably acceptable.

265 Table 3 IOAs of  $O_3$  and  $C_1$ - $C_5$   $\text{RONO}_2$  between simulated and observed values

266

267 Furthermore, the relative contribution of the two reaction pathways, *i.e.* “ $\text{RO}_2 + \text{NO}$ ” and  
 268 “ $\text{RO} + \text{NO}_2$ ”, to the secondary  $\text{RONO}_2$  can be determined with the model running in BC and CC1  
 269 (see model description, section 2.2.2). Taking  $\text{MeONO}_2$  as an example, the reaction of  
 270 “ $\text{CH}_3\text{O}_2 + \text{NO}$ ” and “ $\text{CH}_3\text{O} + \text{NO}_2$ ” contributed  $82.2 \pm 2.5\%$  and  $17.8 \pm 2.5\%$  to the secondary  
 271  $\text{MeONO}_2$ , respectively. This contradicts the hypothesis proposed by [Simpson et al. \(2006\)](#) and  
 272 verified by [Archibald et al. \(2007\)](#), that the reaction of  $\text{CH}_3\text{O}$  and  $\text{NO}_2$  may constitute a major  
 273 part of  $\text{MeONO}_2$  at Tai O. It is well recognized that the most competitive reaction to  
 274 “ $\text{CH}_3\text{O} + \text{NO}_2$ ” is the oxidation of  $\text{CH}_3\text{O}$  by  $\text{O}_2$ , forming  $\text{HCHO}$  and  $\text{HO}_2$ . Here, it was found that  
 275 the reactivity of  $\text{CH}_3\text{O}$  oxidized by  $\text{O}_2$  was approximately four orders of magnitude (*i.e.*  
 276  $\sim 0.8 \times 10^4$ ) higher than that of  $\text{CH}_3\text{O}$  reacting with  $\text{NO}_2$ . On the other hand, the production of  
 277  $\text{HCHO}$  only increased by  $\sim 0.1\%$  when closing off the reaction of “ $\text{CH}_3\text{O} + \text{NO}_2$ ”, suggesting that  
 278 the reaction of  $\text{CH}_3\text{O}$  with  $\text{NO}_2$  is not competitive with the oxidation of  $\text{CH}_3\text{O}$ . **Moreover,**  
 279 **inconsistent with the kinetic calculation by [Simpson et al. \(2006\)](#), the model well reproduced the**  
 280 **secondary  $\text{MeONO}_2$ . It is noteworthy that the branching ratio ( $\alpha$ ) of  $\text{CH}_3\text{O}_2$  reacting with  $\text{NO}$  to**  
 281 **form  $\text{MeONO}_2$  was 0.001 ([Carter and Atkinson, 1989](#)) in MCM protocol, rather than 0.0003**  
 282 **used by [Simpson et al. \(2006\)](#). Additionally,  $\text{CH}_3\text{O}_2$  considered in the kinetic calculations only**  
 283 **involves the OH-initiated oxidation of  $\text{CH}_4$ . Indeed, the sources of  $\text{CH}_3\text{O}_2$  are complicated, *e.g.***  
 284 **photolysis of acetaldehyde and oxidation of  $\text{CH}_4$  by chloride and OH. Model simulations**  
 285 **indicated that OH-initiated oxidation of  $\text{CH}_4$  only contributed  $46.7 \pm 2.9\%$  of  $\text{CH}_3\text{O}_2$  in the**  
 286  **$\text{MeONO}_2$  formation. Namely, the production of  $\text{CH}_3\text{O}_2$  in the kinetic calculation was**  
 287 **underestimated, causing the deficit in  $\text{MeONO}_2$ . [Archibald et al. \(2007\)](#) verified the pathway of**

288 “CH<sub>3</sub>O+NO<sub>2</sub>”, and indicated that it became dominant at NO<sub>2</sub> >35 ppbv. In this study, NO<sub>2</sub>  
289 reached 40.1±5.1 ppbv. However, the contribution of “CH<sub>3</sub>O+NO<sub>2</sub>” to MeONO<sub>2</sub> was not the  
290 foremost (*i.e.*, 17.8±2.5%). Even when the NO<sub>2</sub> level increased by 10 ppbv, the contribution only  
291 increased to 18.7±2.6%. It should be noted that the model Archibald et al. (2007) used was a  
292 simplified version of the MCM 2.0 with a carbon bond mechanism, and the inputs were  
293 European profiles of VOCs and NO<sub>x</sub>, and not the observations in Hong Kong, which may cause  
294 the discrepancies.

295 Based on the source apportionment and pathway contributions to photochemical RONO<sub>2</sub>  
296 formation, the relative contributions of oceanic emissions and possible biomass burning,  
297 “RO<sub>2</sub>+NO” and “RO+NO<sub>2</sub>” can be determined, as shown in Table 4. It was found that the  
298 contribution of oceanic emission and biomass burning decreased from 36.5±6.3% for MeONO<sub>2</sub>  
299 to 26.8±6.8% for 2-PenONO<sub>2</sub>, except for *n*-PrONO<sub>2</sub> (25.8±6.9%), consistent with the  
300 observations in marine outflows. For photochemical formation, the reaction of CH<sub>3</sub>O<sub>2</sub>+NO was  
301 predominant, and the relative contribution increased with increasing carbon number of RONO<sub>2</sub>  
302 except for *n*-PrONO<sub>2</sub>. This is mainly due to the increase of branching ratio leading to RONO<sub>2</sub>  
303 formation from 0.001 for MeONO<sub>2</sub> to 0.131 for 3-PenONO<sub>2</sub>, and to some extent related to the  
304 abundance of RO<sub>2</sub>. For example, the possibility of hydrogen (H) extraction on the second and  
305 third carbon of *n*-pentane is 0.568/0.349 by OH and 0.558/0.220 by chlorine (Cl), causing a  
306 higher contribution of “RO<sub>2</sub>+NO” to 2-PenONO<sub>2</sub> compared to 3-PenONO<sub>2</sub>, although the  
307 branching ratio leading to 2-PenONO<sub>2</sub> formation is slightly lower (0.129). Then, the pathway  
308 contribution of “RO+NO<sub>2</sub>” to MeONO<sub>2</sub> was much higher than that to C<sub>2</sub>-C<sub>5</sub> RONO<sub>2</sub>. This could  
309 be attributable to the abundance of CH<sub>3</sub>O originating from the oxidation of CH<sub>4</sub> and  
310 decomposition of larger RO<sub>2</sub> radicals.

311 Table 4 Pathway contributions to C<sub>1</sub>-C<sub>5</sub> RONO<sub>2</sub> during O<sub>3</sub> episodes at Tai O (unit: %)

312

### 313 3.3 Impact on O<sub>3</sub> formation

#### 314 3.3.1 Net O<sub>3</sub> production

315 RONO<sub>2</sub> chemistry influences the budget of NO<sub>x</sub> and atmospheric radicals, thus influencing the  
316 variations in O<sub>3</sub>. With the model simulation of BC and CC<sub>2</sub> (see model description, 2.2.2), the

317 net O<sub>3</sub> production induced by RONO<sub>2</sub> formation was determined, as shown in Figure 4. Overall,  
318 the RONO<sub>2</sub> formation made negative contributions to O<sub>3</sub>, with the average reduction of  
319 0.05±0.03, 0.05±0.03, 0.06±0.02, 0.02±0.02, 0.18±0.04, 0.09±0.02 and 0.06±0.02 ppbv for the  
320 formation of MeONO<sub>2</sub>, EtONO<sub>2</sub>, *i*-PrONO<sub>2</sub>, *n*-PrONO<sub>2</sub>, 2-BuONO<sub>2</sub>, 2-PenONO<sub>2</sub> and 3-  
321 PenONO<sub>2</sub>, respectively. The average O<sub>3</sub> reduction induced by each RONO<sub>2</sub> formation correlated  
322 well ( $R^2=0.93$ ) with the concentrations of photochemically formed RONO<sub>2</sub>. The average O<sub>3</sub>  
323 reduction rate was  $-11.0\pm 3.2$  ppbv/ppbv. Namely, O<sub>3</sub> was reduced by  $11.0\pm 3.2$  ppbv per ppbv  
324 RONO<sub>2</sub> formation. Although RONO<sub>2</sub> is generally present as a minor constituent (*i.e.* magnitude  
325 of pptv), the effect of RONO<sub>2</sub> formation on O<sub>3</sub> reduction in urban areas cannot be neglected. For  
326 example, on 07 November, 2002, the maximum O<sub>3</sub> reduction caused by the total C<sub>1</sub>-C<sub>5</sub> RONO<sub>2</sub>  
327 reached 2.7 ppbv (~4.4%) at 13:00. On the other hand, not all RONO<sub>2</sub> were considered in this  
328 study due to analytical limitations. Based on the model simulations, the C<sub>1</sub>-C<sub>5</sub> RONO<sub>2</sub>  
329 contributed only 18.6±1.9% of the entire RONO<sub>2</sub> (*i.e.* alkyl and multifunctional nitrates),  
330 implying that the potential of RONO<sub>2</sub> formation on O<sub>3</sub> reduction was underestimated.

331

332 Figure 4 Net O<sub>3</sub> production induced by C<sub>1</sub>-C<sub>5</sub> RONO<sub>2</sub> formation at Tai O

333 To explore the mechanism of O<sub>3</sub> reduction induced by RONO<sub>2</sub> formation, the variation of NO<sub>x</sub>,  
334 HO<sub>x</sub> and the O<sub>3</sub> were studied in detail. Taking 2-BuONO<sub>2</sub> as an example, Figure 5 shows the  
335 temporal variation of each species caused by the formation of 2-BuONO<sub>2</sub>. In general, the OH,  
336 HO<sub>2</sub> and O<sub>3</sub> levels decreased with obvious diurnal variations, while no regular variations were  
337 found for NO<sub>2</sub> and NO. Moreover, the average O<sub>3</sub> reduction rate increased nearly linearly with  
338 the reduction of HO<sub>x</sub> ( $R^2=0.99$ ) and the increase of NO ( $R^2=0.94$ ), suggesting that O<sub>3</sub> formation  
339 was in the VOC-limited regime. Generally, OH consumed by VOC oxidation can be recycled  
340 from the oxidation of RO. However, this pathway was constrained due to the formation of  
341 RONO<sub>2</sub>, therefore the HO<sub>2</sub> and OH generated from the oxidation of RO decreased, and  
342 subsequently O<sub>3</sub> was reduced.

343

344 Figure 5 Variations of NO<sub>2</sub>, NO, HO<sub>2</sub>, OH and O<sub>3</sub> induced by 2-BuONO<sub>2</sub> formation.

345 **3.3.2 Nitrogen partitioning**

346 As a temporary reservoir of nitrogen, RONO<sub>2</sub> contributes to O<sub>3</sub> production in downwind  
347 regions through the release of NO<sub>2</sub>. Therefore, quantifying the role of RONO<sub>2</sub> in the nitrogen  
348 budget is essential to estimating its impact on O<sub>3</sub> production in remote areas. Figure 6 shows the  
349 mixing ratios of sinks (*i.e.* HNO<sub>3</sub>) and temporary reservoirs (*i.e.* PANs, RONO<sub>2</sub>, N<sub>2</sub>O<sub>5</sub> and NO<sub>3</sub>)  
350 of nitrogen, as simulated by the PBM-MCM model. It is noteworthy that the entire RONO<sub>2</sub>  
351 included alkyl and multifunctional nitrates here, PANs included the total peroxyacyl nitrates, and  
352 HONO was not considered as it decomposes quickly in the daytime. It was found that PANs,  
353 RONO<sub>2</sub> and HNO<sub>3</sub> increased from the morning and reached their maximums in the afternoon or  
354 at dusk. As the most important nitrogen reservoirs, PANs, RONO<sub>2</sub> and HNO<sub>3</sub> accounted for  
355 53.0±4.1%, 29.8±4.9% and 12.8±0.5% of the total reserved nitrogen, respectively. For NO<sub>3</sub> and  
356 N<sub>2</sub>O<sub>5</sub>, they began to build up from the late afternoon (*i.e.* 16:00-17:00) due to their poor  
357 stabilities in sunlight, constituting 0.5±0.3% and 3.9±2.0% of the total reserved nitrogen,  
358 respectively.

359 It is noticeable that variations of the entire RONO<sub>2</sub> was consistent with those of the C<sub>1</sub>-C<sub>5</sub>  
360 RONO<sub>2</sub> (see Figure 3), indicating similar formation mechanisms for all RONO<sub>2</sub>. The C<sub>1</sub>-C<sub>5</sub>  
361 RONO<sub>2</sub> accounted for 18.6±1.9% of the entire RONO<sub>2</sub>, which means that 4.1±0.2% nitrogen  
362 was stored in the C<sub>1</sub>-C<sub>5</sub> RONO<sub>2</sub>. It should be noted that most RONO<sub>2</sub> have much longer lifetimes  
363 than PANs, causing longer and higher O<sub>3</sub> formation in the remote atmosphere due to the  
364 transport of RONO<sub>2</sub> and continual release of NO<sub>2</sub>. This needs further study, beyond the scope of  
365 the present work, for example by undertaking continuous sampling in both the upwind (*i.e.*  
366 RONO<sub>2</sub> formation) and downwind (*i.e.* RONO<sub>2</sub> degradation) regions.

367

368 Figure 6 Time series of reserved nitrogen at daytime hours on episode days at Tai O

369

## 370 4. Conclusions

371 In this study, data from a comprehensive field measurement campaign, conducted from  
372 August 2001 to December 2002 at Tai O, a coastal site in Hong Kong, was used to investigate  
373 the pathways leading to C<sub>1</sub>-C<sub>5</sub> RONO<sub>2</sub> and their impacts on O<sub>3</sub> formation. The sum of C<sub>1</sub>-C<sub>5</sub>  
374 RONO<sub>2</sub> were the highest in autumn and correlated well with O<sub>3</sub>, suggesting the importance of

375 photochemical formation. Evaluation of the Hong Kong PBM-MCM model constrained with the  
376 field data gave good to moderate agreement between observed and simulated secondary C<sub>1</sub>-C<sub>5</sub>  
377 RONO<sub>2</sub> and O<sub>3</sub>. The model was further applied to quantify the contribution of each pathway to  
378 C<sub>1</sub>-C<sub>5</sub> RONO<sub>2</sub>. In contrast with previous suggestions, the reaction of CH<sub>3</sub>O with NO<sub>2</sub> was not the  
379 major pathway for MeONO<sub>2</sub> formation, accounting for only 11.3±0.7% of the total MeONO<sub>2</sub>,  
380 while the pathway of CH<sub>3</sub>O<sub>2</sub> reacting with NO and oceanic emission /biomass burning  
381 contributed 51.8±3.1% and 36.5±6.3% to the total MeONO<sub>2</sub>, respectively. From EtONO<sub>2</sub> to  
382 PenONO<sub>2</sub>, the contribution to RONO<sub>2</sub> made by photochemical formation increased, while that of  
383 oceanic/biomass burning emissions decreased. Studies on the relationship between net O<sub>3</sub>  
384 production and RONO<sub>2</sub> formation indicated that RONO<sub>2</sub> formation limited O<sub>3</sub> formation due to  
385 the decrease of OH and HO<sub>2</sub>. The average O<sub>3</sub> reduction rate was -11.0±3.2 ppbv O<sub>3</sub> per ppbv  
386 RONO<sub>2</sub>. Although RONO<sub>2</sub> is a minor component of NO<sub>y</sub>, the impact of total RONO<sub>2</sub> on O<sub>3</sub>  
387 reduction cannot be neglected. Moreover, the nitrogen reserved in RONO<sub>2</sub> (4.1±0.2%) may  
388 continue to contribute to O<sub>3</sub> formation in downwind areas. These findings enhance our  
389 knowledge on the influence of individual RONO<sub>2</sub> species on O<sub>3</sub> production.

## 390 Acknowledgements

391 This study was supported by the Research Grants Council of the Hong Kong Special  
392 Administrative Region via grants PolyU5154/13E and PolyU152052/14E, and the Hong Kong  
393 Polytechnic University Ph.D. scholarships (project #RTUP). This study is partly supported by  
394 the Public Policy Research Funding Scheme (2013.A6.012.13A) and the National Natural  
395 Science Foundation of China (No. 41405112). We appreciate Prof. Blake's group at the  
396 University of California at Irvine for the chemical analysis of the whole air VOC samples.

397

## 398 References

- 399 Archibald, A.T., Khan, M.A.H., Watson, L.A., Utembe, S.R., Shallcross, D.E., Clemitshaw, K.C., Jenkin,  
400 M.E., 2007. Comment on 'Long-term atmospheric measurements of C<sub>1</sub>-C<sub>5</sub> alkyl nitrates in the Pearl  
401 River Delta region of southeast China' by Simpson et al.. Atmos. Environ. 41, 7369-7370.
- 402 Aruffo, E., Carlo, P.D., Dari-Salisburgo, C., Biancofiore, F., Giammaria, F., Busilacchio, M., Lee, J.,  
403 Moller, S., Hopkins, J., Punjabi, S., Bauguitte, S., O'Sullivan, D., Percival, C., Breton, M.L., Muller, J.,  
404 Jones, R., Forster, G., Reeves, C., Heard, D., Walker, H., Ingham, T., Vaughan, S., Stone, D., 2014.

- 405 Aircraft observations of the lower troposphere above a megacity: Alkyl nitrate and O<sub>3</sub> chemistry.  
406 Atmos. Environ. 94, 479-488.
- 407 Aschmann, S.M., Tuazon, E.C., Arey, J., Atkinson, R., 2011. Products of the OH radical-initiated  
408 reactions of 2-propyl nitrate, 3-methyl-2-butyl nitrate and 3-methyl-2-pentyl nitrate. Atmos. Environ.  
409 45, 1695-1701.
- 410 Atkinson, R., Aschmann, S.M., Carter, W.P.L., Winer, A.M., Pitts, J.N., 1982. Alkyl nitrate formation  
411 from the nitrogen oxide (NO<sub>x</sub>)-air photooxidations of C<sub>2</sub>-C<sub>8</sub> n-alkanes. J. Phys. Chem. 86, 4563-4569.
- 412 Atkinson, R., Carter, W.P.L., Winer, A.M., 1983. Effects of Temperature and Pressure on Alkyl Nitrate  
413 Yields in the NO<sub>x</sub> Photooxidations of +Pentane and n-Heptane. J. Phys. Chem. 87, 2012-2018.
- 414 Atlas, E., 1988. Evidence for ≥C<sub>3</sub> alkyl nitrates in rural and remote atmospheres. Nature 331, 426-428.
- 415 Atlas, E., Pollock, W., Greenberg, J., Heidt, L., Thompson, A.M., 1993. Alkyl nitrates, nonmethane  
416 hydrocarbons, and halocarbon gases over the equatorial Pacific Ocean during SAGA-3, J. Geophys.  
417 Res. 98, 16933-16947.
- 418 Blake, N.J., Blake, D.R., Swanson, A.L., Atlas, E., Flocke, F., Rowland, F.S., 2003. Latitudinal, vertical  
419 and seasonal variations of the C<sub>1</sub>-C<sub>4</sub> alkyl nitrates in the troposphere over the Pacific Ocean during  
420 PEM-Tropics A and B: Oceanic and continental sources. J. Geophys. Res. 108, 8284,  
421 <http://dx.doi.org/10.1029/2001JD001444>.
- 422 Cheng, H.R., Guo, H., Saunders, S.M., Lam, S.H.M., Jiang, F., Wang, X.M., Simpson, I.J., Blake, D.R.,  
423 Louie, P.K.K., Wang, T.J., 2010. Assessing photochemical O<sub>3</sub> formation in the Pearl River Delta with a  
424 photochemical trajectory model. Atmos. Environ. 44, 4199-4208.
- 425 Colman, J.J., Swanson, A.L., Meinardi, S., Sive, B.C., Blake, D.R., Rowland, F.S., 2001. Description of  
426 the analysis of a wide range of volatile organic compounds in whole air samples collected during PEM-  
427 Tropics A and B. Anal. Chem. 73, 3723-3731.
- 428 Derwent, R.G., Jenkin, M.E., Saunders, S.M., Pilling, M.J., Passant, N.R., 2005. Multi-day O<sub>3</sub> formation  
429 for alkenes and carbonyls investigated with a master chemical mechanism under European conditions.  
430 Atmos. Environ. 39, 627-635.
- 431 Farmer, D.K., Perring, A.E., Wooldridge, P.J., Blake, D.R., Baker, A., Meinardi, S., Huey, L.G., Tanner,  
432 D., Vargas, O., Cohen, R.C., 2011. Impact of organic nitrates on urban O<sub>3</sub> production. Atmos. Chem.  
433 Phys. 11, 4085-4094.
- 434 Flocke, F., Volz-Thomas, A., Buers, H.J., Patz, W., Garthe, H.J., Kley, D., 1998. Long-term  
435 measurements of alkyl nitrates in southern Germany 1. General behavior and seasonal and diurnal  
436 variation. J. Geophys. Res. 103, 5729-5746.
- 437 Guo, H., Cheng, H.R., Ling, Z.H., Louie, P.K.K., Ayoko, G., 2011. Which emission sources are  
438 responsible for the volatile organic compounds in the atmosphere of Pearl River Delta?. J. Hazard.  
439 Mater. 188, 116-124.
- 440 Guo, H., Ling, Z.H., Cheung, K., Jiang, F., Wang, D.W., Simpson, I.J., Barletta, B., Meinardi, S., Wang,  
441 T.J., Wang, X.M., Saunders, S.M., Blake, D.R., 2013a. Characterization of photochemical pollution at  
442 different elevations in mountainous areas in Hong Kong. Atmos. Chem. Phys. 13, 3881-3898.

- 443 Guo, H., Ling, Z.H., Cheung, K., Wang, D.W., Simpson, I.J., Blake, D.R., 2013b. Acetone in the  
444 atmosphere of Hong Kong: Abundance, sources and photochemical precursors. *Atmos. Environ.* 65,  
445 80-88.
- 446 Guo, H., So, K.L., Simpson, I.J., Barletta, B., Meinardi, S., Blake, D.R., 2007. C<sub>1</sub>-C<sub>8</sub> volatile organic  
447 compounds in the atmosphere of Hong Kong: Overview of atmospheric processing and source  
448 apportionment. *Atmos. Environ.* 41, 1456-1472.
- 449 He, S.Z., Chen, Z.M., Zhang, X., 2011. Photochemical reactions of methyl and ethyl nitrate: a dual role  
450 for alkyl nitrates in the nitrogen cycle. *Environ. Chem.* 8, 529-542.
- 451 Huang, J.P., Fung, J.C.H., Lau, A.K.H., Qin, Y., 2005. Numerical simulation and process analysis of  
452 typhoon-related O<sub>3</sub> episodes in Hong Kong. *J. Geophys. Res.* 110,  
453 <http://dx.doi.org/10.1029/2004JD004914>.
- 454 Jenkin, M.E., Clemitshaw, K.C., 2000. Ozone and other secondary photochemical pollutants: chemical  
455 processes governing their formation in the planetary boundary layer. *Atmos. Environ.* 34, 2499-2527.
- 456 Jenkin, M.E., Saunders, S.M., Wagner, V., Pilling, M.J., 2003. Protocol for the development of the  
457 Master Chemical Mechanism, MCM v3 (Part B): tropospheric degradation of aromatic volatile organic  
458 compounds. *Atmos. Chem. Phys.* 3, 181-193.
- 459 Jiang, F., Guo, H., Wang, T.J., Cheng, H.R., Wang, X.M., Simpson, I.J., Ding, A.J., Saunders, S.M., Lam,  
460 S.H.M., Blake, D.R., 2010. An O<sub>3</sub> episode in the Pearl River Delta: Field observation and model  
461 simulation. *J. Geophys. Res.* 115, <http://dx.doi.org/10.1029/2009JD013583>.
- 462 Lam, S.H.M., Saunders, S.M., Guo, H., Ling, Z.H., Jiang, F., Wang, X.M., Wang, T.J., 2013. Modelling  
463 VOC source impacts on high ozone episode days observed at a mountain summit in Hong Kong under  
464 the influence of mountain-valley breezes. *Atmos. Environ.* 81, 166-176.
- 465 Ling, Z.H., Guo, H., Cheng, H.R., Yu, Y.F., 2011. Sources of ambient volatile organic compounds and  
466 their contributions to photochemical O<sub>3</sub> formation at a site in the Pearl River Delta, southern China.  
467 *Environ. Pollut.* 159, 2310-2319.
- 468 Ling, Z.H., Guo, H., Lam, S.H.M., Saunders, S.M., Wang, T., 2014. Atmospheric photochemical  
469 reactivity and ozone production at two sites in Hong Kong: Application of a Master Chemical  
470 Mechanism-photochemical box model. *J. Geophys. Res. Atmos.* 119, 10567-10582.
- 471 Madronich, S., Flocke, S., 1997. Theoretical estimation of biologically effective UV radiation at the  
472 Earth's surface. In: Zerefos, C. (Ed.), *Solar Ultraviolet Radiation-Modeling, Measurements and Effects*,  
473 NATO ASI Series, vol. I52. Springer-Verlag, Berlin.
- 474 Nowak, J.B., Davis, D.D., Chen, G., Eisele, F.L., Mauldin III, R.L., Tanner, D.J., Cantrell, C., Kosciuch,  
475 E., Bandy, A., Thornton, D., Clarke, A., 2001. Airborne observations of DMSO, DMS, and OH at  
476 marine tropical latitudes. *Geophys. Res. Lett.* 28, 2201-2204.
- 477 Paatero, P., 1997. Least squares formulation of robust non-negative factor analysis. *Chemom. Intell. Lab.*  
478 *Sys.* 37, 23-35.
- 479 Saunders, S.M., Jenkin, M.E., Derwent, R.G., Pilling, M.J., 2003. Protocol for the development of the  
480 Master Chemical Mechanism, MCM v3 (Part A): tropospheric degradation of non-aromatic volatile  
481 organic compounds. *Atmos. Chem. Phys.* 3, 161-180.



- 482 Simpson, I.J., Akagi, S.K., Barletta, B., Blake, N.J., Choi, Y., Diskin, G.S., Fried, A., Fuelberg, H.E.,  
483 Meinardi, S., Rowland, F.S., Vay, S.A., Weinheimer, A.J., Wennberg, P.O., Wiebring, P., Wisthaler,  
484 A., Yang, M., Yokelson, R.J., Blake, D.R., 2011. Boreal forest fire emissions in fresh Canadian smoke  
485 plumes: C<sub>1</sub>-C<sub>10</sub> volatile organic compounds (VOCs), CO<sub>2</sub>, CO, NO<sub>2</sub>, NO, HCN and CH<sub>3</sub>CN. *Atmos.*  
486 *Chem. Phys.* 11, 6445-6463.
- 487 Simpson, I.J., Meinardi, S., Blake, D.R., Blake, N.J., Rowland, F.S., Atlas, E., Flocke, F., 2002. A  
488 biomass burning source of C<sub>1</sub>-C<sub>4</sub> alkyl nitrates. *Geophys. Res. Lett.* 29(24), 2168,  
489 <http://doi:10.1029/2002GL016290>.
- 490 Simpson, I.J., Wang, T., Guo, H., Kwok, Y.H., Flocke, F., Atlas, E., Meinardi, S., Rowland, F.S., Blake,  
491 D.R., 2006. Long-term atmospheric measurements of C<sub>1</sub>-C<sub>5</sub> alkyl nitrates in the Pearl River Delta  
492 region of southeast China. *Atmos. Environ.* 40, 1619-1632.
- 493 Symth, S., Bradshaw, J., Sandholm, S., Liu, S., Mckeen, S., Gregory, G., Anderson, B., Talbot, R., Blake,  
494 D., Rowland, S., Browell, E., Fenn, M., Merrill, J., Backmeier, S., Sachse, G., Collins, J., Thornton, D.,  
495 Davis, D., Singh, H., 1996. Comparison of free tropospheric western Pacific air mass classification  
496 schemes for the PEM-West A experiment. *J. Geophys. Res.* 101, 1743-1762.
- 497 Suarez-Bertoa, R., Picquet-Varrault, B., Tamas, W., Pangui, E., Doussin, J.F., 2012. Atmospheric Fate of  
498 a Series of Carbonyl Nitrates: Photolysis Frequencies and OH-Oxidation Rate Constants. *Environ. Sci.*  
499 *Technol.* 46, 12502-12509.
- 500 Wang, M., Shao, M., Chen, W.T., Lu, S.H., Wang, C., Huang, D.K., Yuan, B., Zeng, L.M., Zhao, Y.,  
501 2013. Measurements of C<sub>1</sub>-C<sub>4</sub> alkyl nitrates and their relationships with carbonyl compounds and O<sub>3</sub> in  
502 Chinese cities. *Atmos. Environ.* 81, 389-398.
- 503 Wang, N., Guo, H., Jiang, F., Ling, Z.H., Wang, T., 2015. Simulation of O<sub>3</sub> formation at different  
504 elevations in mountainous area of Hong Kong using WRF-CMAQ model. *Sci. Total Environ.* 505,  
505 939-951.
- 506 Wang, T., Guo, H., Blake, D.R., Kwok, Y.H., Simpson, I.J., Li, Y.S., 2005. Measurements of Trace Gases  
507 in the Inflow of South China Sea Background Air and Outflow of Regional Pollution at Tai O,  
508 Southern China. *J. Atmos. Chem.* 52, 295-317.
- 509 Wang, T., Poon, C.N., Kwok, Y.H., Li, Y.S., 2003. Characterizing the temporal variability and emission  
510 patterns of pollution plumes in the Pearl River Delta of China. *Atmos. Environ.* 37, 3539-3550.
- 511 Wang, T., Wei, X.L., Ding, A J., Poon, C.N., Lam, K.S., Li, Y.S., Chan, L.Y., Anson, M., 2009.  
512 Increasing surface O<sub>3</sub> concentrations in the background atmosphere of Southern China, 1994-2007.  
513 *Atmos. Chem. Phys.* 9, 6217-6227.
- 514 Williams, J.E., Bras, G.L., Kukui, A., Ziereis, H., Brenninkmeijer, A.M., 2014. The impact of the  
515 chemical production of methyl nitrate from the NO + CH<sub>3</sub>O<sub>2</sub> reaction on the global distributions of  
516 alkyl nitrates, nitrogen oxides and tropospheric O<sub>3</sub>: a global modelling study. *Atmos. Chem. Phys.* 14,  
517 2363-2382.
- 518 Worton, D.R., reeves, C.E., Penkett, S.A., Sturges, W.T., Slemr, J., Oram, D.E., Bandy, B.J., Bloss, W.J.,  
519 Carslaw, N., Davey, J., Emmerson, K.M., Gravestock, T.J., Hamilton, J.F., Heard, D.E., Hopkins, J.R.,  
520 Hulse, A., Ingram, T., Jacob, M.J., Lee, J.D., Leigh, R.J., Lewis, A.C., Monks, P.S., Smith, S.C., 2010.  
521 Alkyl nitrate photochemistry during the tropospheric organic chemistry experiment. *Atmos. Environ.*  
522 44, 773-785.

523 Xu, Z., Wang, T., Xue, L.K., Louie, P.K.K., Luk, C.W.Y., Gao, J., Wang, S.L., Chai, F.H., Wang, W.X.,  
524 2013. Evaluating the uncertainties of thermal catalytic conversion in measuring atmospheric nitrogen  
525 dioxide at four differently polluted sites in China. *Atmos. Environ.* 76, 221-226.